Length vs Stiffness, Which Plays a Dominant Role in the Cellular Uptake of Fructose-based Rod-like Micelles by Breast Cancer Cells in 2D and 3D Cell Culture Models?

Journal:	*Journal of Materials Chemistry B*
Manuscript ID	TB-ART-03-2018-000706.R2
Article Type:	Paper
Date Submitted by the Author:	14-May-2018
Complete List of Authors:	Zhao, Jiacheng; University of New South Wales, School of Chemical Sciences and Engineering Lu, Hongxu; University of New South Wales, Yao, Yin; University of New South Wales, Materials Science and Engineering Ganda, Sylvia; UNSW, chemistry Stenzel, Martina; University of New South Wales, School of Chemistry

SCHOLARONE™
Manuscripts

Journal Name

ARTICLE

Length vs Stiffness, Which Plays a Dominant Role in the Cellular Uptake of Fructose-based Rod-like Micelles by Breast Cancer Cells in 2D and 3D Cell Culture Models?

Jiacheng Zhao,[a,b] Hongxu Lu,[a,b] Yin Yao,[c] Sylvia Ganda,[a,b] and Martina H. Stenzel † [a,b]

Polymeric nanoparticles with long circulation time hold great promise for anti-cancer drug delivery. Enhanced circulation effect of rod-like micelles has been reported, yet efficient intracellular delivery, especially their interactions with cells during endocytosis still remains inconsistent. Internalization of rod-like nanoparticles is significantly affected by a number of factors including aspect ratio, stiffness and surface chemistry of nanoparticles. Our former research shows that the length of rods affected their cellular uptake by breast cancer cells. Here, the influence of rod stiffness in cellular uptake was investigated to provide a comprehensive understanding of the interaction between rods and cells during endocytosis. Well-defined fructose-coated rod-like micelles of different lengths and stiffness were prepared successfully. AFM results indicate that rods based on Poly(1-O-MAFru)$_{31}$-b-PMMA$_{166}$ are significantly stiffer than those prepared from Poly(1-O-MAFru)$_{31}$-b-PBA$_{158}$. Cellular uptake of these different rod-like micelles by breast cancer cells was investigated. In vitro studies via 2D and 3D cell culture models reveal that the stiffer rods have a higher cellular uptake and a deeper penetration into the cell compared to the soft rod-like micelles. These results indicate that the internalization of rod-like micelles is significantly affected by their stiffness, though the length of rods also plays an important role. Our results yield fundamental understanding of the stiffness effect of rod-like micelles on cellular uptake.

Introduction

Polymeric nanoparticle-based diagnostic and therapeutic agents have been considered as a promising platform for anti-cancer therapy due to their high targeting specificity and efficiency.[1] The delivery of bioagents can be well controlled by tailoring the size,[2-5] shape,[6-8] and surface chemistry[9, 10] of nanocarriers to achieve optimized therapeutic efficacy. Compared to spherical drug nanocarriers, some rod-like nanoparticles are reported to have enhanced drug delivery efficiency,[11] reduced toxicity to body,[12] prolonged blood circulation time and good selectivity to cancer cells.[13] Extensive efforts have been made to understand the effect of nanoparticle shape on cellular uptake.[14-16] However, most of the available results lack consistence relating to the cellular uptake of elongated nanoparticles like filaments or rods compared to spherical nanoparticles. For instance, inhibited endocytosis of rod-like nanoparticles by macrophages and cancer cells has been extensively reported. Negligible phagocytosis of polystyrene worms was observed by Champion *et al*.[17] Rod-like hydrogel was also reported to be taken up by HeLa cells to a lower extent than spherical counterparts.[8] Wooley's group investigated the cellular uptake of TAT-HIV protein functionalized spheres and rods by Chinese Hamster Ovary (CHO) cells.[6] Their results indicated that the endocytosis rate of rods was much lower than that of spherical nanoparticles. At the same time, enhanced uptake of rod-like micelles compared to spherical micelles has been reported frequently.[18-21] Therefore, no conclusions can be drawn in regards to the preferred shape for cellular uptake as most of the reported results are based on different cell lines, nanoparticles with different surface chemistry and rod-like micelles of various aspect ratios. While the effect of some of these parameters is discussed, the intrinsic properties of rod-like micelles are often neglected. Actually elastic modulus was reported to significantly affect the biodistribution and circulation times of hydrogel microparticles in vivo.[22] It is feasible that parameters such as the softness of the rod may play a considerable role and the investigation of the effect of stiffness or softness on the cellular uptake is therefore significant.

Aim of this work is therefore to evaluate the cellular uptake of non-spherical nanoparticles in dependency on hardness of the material. We have therefore prepared cylindrical micelles based on fructose, which are promising drug nano-carriers for triple-negative breast cancer therapy.[5, 23, 24] These glycopolymer-micelles exhibited excellent breast cancer cell-specific uptake due to interaction between fructose moieties and GLUT5 expressed by breast cancer cells. The cellular uptake of fructose-based rod-like micelles in breast cancer cell models revealed a decline in uptake with increasing aspect ratio.[25] Considering the endocytic pathways of nanoparticle where nanoparticles are engulfed into the cell by endocytic pits of typically 100-200 nm in size,[26] the length, but also the flexibility of rod-like nanoparticles, which often exceed the size of the pit by several orders should play a significant role. We have therefore studied here the effect of the rod length and stiffness on cellular uptake to shine light on the understanding of the endocytosis mechanism of rod-like nanoparticles. To complement the study, the movement of these nanoparticles in multicellular spheroid models has been studies as it has been shown that endo- and exocytosis affect the rate of penetration into the 3D model.[27] The nanoparticles were prepared by self-assembly of block copolymers based on Poly(1-O-methacryloyl -β-D-fructopyranose) (1-O-MAFru) as the hydrophilic block while the hydrophobic block was either based on poly(methyl methacrylate), a polymer with high glass transition temperature T_g, or poly(n-butyl acrylate) PBA, which has a T_g below room temperature.

Experimental

Materials

D-fructose (99%, Aldrich), dichloromethane (DCM; anhydrous, >99.8%, Aldrich), methacrylic anhydride (94%, Aldrich), 4-dimethylaminopyridine (DMAP; 94%, Aldrich), sulfuric acid (95%-98%, Ajax Finechem), acetone (HPLC grade, Ajax Finechem), tetrahydrofuran (THF; 99%, Ajax Finechem), fluorescein O-methacrylate (97%, Aldrich) and N,N-dimethylformamide (DMF; 99%, Ajax Finechem) were used as received. 1,4-dioxane (99%, Ajax Finechem) and pyridine (99%, Ajax Finechem) were purified by reduced-pressure distillation. Methyl methacrylate (>99%, Aldrich) was passed over basic aluminium oxide to remove the inhibitors. 2,2-azobis(isobutyronitrile) (AIBN; 98%, Fluka) was recrystallized from methanol for purification. The RAFT agent 4-cyanopentanoic acid dithiobenzoate (CPADB) was synthesized according to a literature procedure.[28] The synthesis of 1-O-methacryloyl-2,3:4,5-di-O-isopropylidene-β-D-fructopyranose (1-O-MAipFru) as well as the block copolymers are described in detail elsewhere.[25]

Synthesis and methods

Synthesis of Poly(1-O-MAFru) -b-PBA. A typical procedure was described as follows: in a Schlenk tube, 1-O-methacryloyl-2,3:4,5-di-O-isopropylidene-β-D-fructopyranose (1 g, 3.05 mmol), fluorescein O-methacrylate (70 mg, 0.185mmol), AIBN

(1.33 mg, 8.1×10^{-3} mmol) and CPADB (17 mg, 0.061 mmol) were dissolved in 1,4-dioxane (4.3 mL). Then the tube was degassed by three freeze-pump-thaw cycles. The polymerization was carried out at 70 ℃ and stopped at 7 h by cooling the solution in ice water. The polymer solution was poured into a large excess of diethyl ether for precipitation. The solid was dried under vacuum for 24 h. The obtained polymer was then used as macro RAFT agent for the following chain extension. A typical procedure for the synthesis of Poly(1-O-MAFru)$_{31}$-b-PBA$_{158}$ was described as follows: macro RAFT agent (200 mg, 2×10^{-2} mmol), n-butyl acrylate (640 mg, 5 mmol), AIBN (0.64 mg, 4×10^{-3} mmol) and fluorescein O-methacrylate (14 mg, 0.037mmol) were dissolved in 1,4-dioxane (3 mL). The tube was degassed by three freeze-vacuum-thaw cycles. The polymerization was carried out at 70 ℃ and stopped at 18 h by cooling the solution in ice water. The polymer solution was poured into a large excess of n-hexane for precipitation. The viscous polymer was dried under vacuum for 24 h. The deprotection of the block copolymers was carried out under acidic conditions. The polymer (80 mg) was added into 1.59 mL of TFA/H$_2$O (9:1 v/v) in a vial with stirring at room temperature for 30 minutes. After reaction, the polymer solution was dialyzed against deionized water for two days (MWCO 3500). The deprotected polymer was then lyophilized.

Synthesis of Poly(1-O-MAFru) -b-PMMA. The synthesis of macro RAFT agent was described as above. The chain extension was carried out like this: macro RAFT agent (200 mg, 2×10^{-2} mmol), methyl methacrylate (516 mg, 5.16 mmol), AIBN (0.64 mg, 4×10^{-3} mmol) and fluorescein O-methacrylate (14 mg, 0.037mmol) were dissolved in 1,4-dioxane (3 mL) at first. The solution was degassed by three freeze-vacuum-thaw cycles and reacted at 70 ℃ for 18 h. A large excess of n-hexane was used for precipitation. The viscous polymer was dried under vacuum for 24 h. The deprotection of the block copolymers was carried out under acidic conditions. The polymer (80 mg) was added into 1.59 mL of TFA/H2O (9:1 v/v) in a vial with stirring at room temperature for 30 minutes. After reaction, the polymer solution was dialyzed against deionized water for two days (MWCO 3500). The deprotected polymer was then lyophilized.

Self-assembly of block glycopolymers. Deprotected polymer (4 mg) was dissolved in THF (0.2 mL). Then 1.8 mL MQ water was added to the polymer solution using a syringe pump with a rate of 0.2 mL/h. A glass cooling tube was used to control the temperature of solution precisely and tempering medium was pumped around the double walled vessel. The stirring rate was controlled by a heating plate. The micelle solution was dialyzed against deionized water to remove THF.

Transmission electron microscopy (TEM). The TEM micrographs were obtained using a JEOL1400 transmission electron microscope comprising of a dispersive X-ray analyzer and a Gatan CCD facilitating the acquisition of digital images. The measurement was conducted at an accelerating voltage of 80 kV. The samples were prepared by casting the micellar solution

(1 mg/mL) onto a copper grid. The grids were dried by air and then negatively stained with uranyl acetate.

Atomic Force Microscopy (AFM). The moduli of rods were measured using a Bruker Dimension SPM ICON atomic force microscopy. For normal topological imaging, the TAP150A/RTESPA-150 probe (6 N/m spring constant, 150 kHz resonance frequency) was used for both nano-particle samples. The probe was firstly tuned with target amplitude of 300mV, which gave about 15nm free oscillation amplitude. The scan rate was set to 0.35 to 0.5 Hz and the scan size is 2 µm. For peakforce QNM, two types of AFM probes supplied by Bruker were used. The RTESPA-150 is used for the PBA sample. The OTESPA-R3 probe (spring constant of 28 N/m and a resonance frequency of around 300 kHz) was used for PMMA because it is much stiffer than the PBA sample. For reliable mechanical measurements, the probe needs to be calibrated. Firstly, the deflection sensitivity was calculated by engaging the probe onto a clean quartz sample. Afterwards, the spring constant of the probe was calculated by thermal tuning. Finally, the tip end radius of the probe is measured by imagining a titanium tip checker. Because the titanium roughness sample is very sharp and can easily damage the probe, a slow scan rate of 0.25 Hz was used. The peakforce setpoint was adjusted as low as possible in order to minimize damage to the tip. After imagining the tip checker, the nano-particle sample was measured at a scan rate of 0.35 Hz. The scan size was set to 2 µm. In order to ensure accurate results, multiple images were taken and a new probe was loaded for each new sample. In addition, after scanning, the AFM tip was regularly checked with SEM to ensure the tip is still sharp and free of contamination.

Fluorescence Spectroscopy. The fluorescence properties of micelles were studied using the Cary Eclipse Fluorescence Spectrophotometer (Agilent Technologies). The concentration of the micelle solution was 200 µg/mL.

Dynamic Light Scattering (DLS). Particle sizes (average hydrodynamic diameters and size distributions) were determined using a Malvern Zetaplus particle size analyzer (4 mV He-Ne laser, 35mW, λ = 632 nm, noninvasive backscatter detection at 173°) at a polymer concentration of 1.0 mg/mL.

3D Multicellular Tumor Spheroids (MCTS) Formation. The MCTS were prepared by a liquid overlay method as follows: MCF-7 cells were suspended in cell growth medium at a density of 1×10^4 cells/mL. 200 µL of the cell suspension was seeded into each well of ultralow attachment U-bottom 96-well plate (Corning) and incubated for 3 days. Cells would aggregate and form MCTSs with a diameter about 400 µm. Micelle solutions were loaded into the microplate and incubated for 12 h before the observation with confocal microscopy.

Flow Cytometry. Cellular uptake was measured using a flow cytometer (BD FACSort). Breast cancer cells (MCF-7 cells and MDA-MB-231 cells) were seeded in 6-well tissue culture polystyrene plates at a density of 5×10^5 cells per well in 3 mL culture medium. After 24 hours, the medium was then replaced with 2-time fresh medium (1000 µL) and 1000 µL micelle solution with a concentration of 200 µg/mL and incubated in the same conditions for 12 h. After incubation, the cells were then washed thrice with cold PBS, collected by trypsin/EDTA treatment and resuspended in cold Hank's balanced salt solution. The cell suspension was measured using the BD FACSort flow cytometer. Non-treated cells were used as controls. All uptake tests were replicated thrice in an individual experiment.

Laser Scanning Confocal Microscopy. Cells (MCF-7 cells and MDA-MB-231 cells) were seeded in 35 mm Fluorodishes (World Precision Instruments) at a density of 5×10^5 cells per well in 3 mL Dulbecco's modified Eagle's medium (DMEM) supplemented with 2.2 g/L NaHCO$_3$, 10% (v/v) foetal bovine serum (FBS), 100 U/mL penicillin and 100 µg/mL streptomycin. Micelles were loaded to the cells at a working concentration of 100 µg/mL and incubated in a humidified incubator (5% CO$_2$/ 95% air atmosphere at 37 °C) for 12 h. After incubation, the cells were washed thrice with PBS, and then stained with 2.0 µg/mL Hoechst 33342 (Invitrogen) for 5 min. Finally, 100 nM Lyso Tracker Red DND-99 (Invitrogen) for 1 min. 3D Multicellular Tumor spheroids were prepared as described above. After incubation for 3 days, micelles were loaded and incubated for 12 h. After incubation, the spheroids were washed thrice with PBS and finally mounted in PBS for imaging. A laser scanning confocal microscope system (Zeiss LSM 780) consisted of a Diode 405-30 laser, an argon laser and a DPSS 56110 laser (excitation and absorbance wavelengths: 405, 448 and 561 nm) connected to a Zeiss Axio Observer.Z1 inverted microscope (oil immersion ×100/1.4 NA objective) was used for observation. The Zen2011 imaging software (Zeiss) was used for imaging acquisition and processing. All uptake tests were replicated thrice in an individual experiment.

Results and discussion
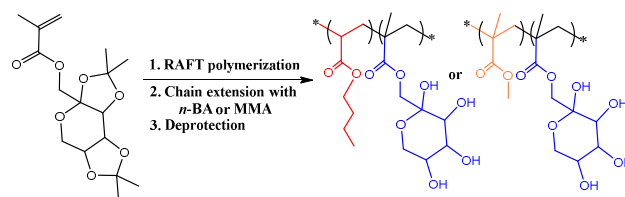
Scheme 1. Synthesis of fructose-based amphiphilic block glycopolymers.

Fructose-based block copolymers with different hydrophobic blocks, but the same glycopolymer block lengths, were synthesized as shown in Scheme 1. Poly(1-*O*-MAipFru)$_{31}$ was synthesized and used as macro-CTA for the further chain extension with the hydrophobic monomers. To obtained rod-like micelles with different stiffness, *n*-butyl acrylate (BA) and methyl methacrylate (MMA) were selected to obtain glycopolymers with low *Tg* (*Tg*$_{[PBA]}$ = ~ -40 °C) and high *Tg* (*Tg*$_{[PMMA]}$ = ~ 80-105 °C). As demonstrated in Table 1 and Figure

S1, the chain extension with BA and MMA were carried out in a controlled manner and the molecular weight distribution of the obtained glycopolymers are narrow ($Đ$ < 1.2). The removal of isopropylidene groups was conducted under acidic conditions, followed by dialysis and lyophilization before micelle preparation.

Table 1. Synthesis of block glycopolymers via RAFT Polymerization at 70℃ in 1,4-dioxane.

Glycopolymers	[M]:[Macro-CTA]:[AIBN]	Conversion (%)	Mn /g.mol^{-1} (SEC)	$Đ$ (SEC)
Poly(1-O-MAipFru)$_{31}$-b-PMMA$_{166}$	260 : 1 : 0.2	63	38900	1.15
Poly(1-O-MAipFru)$_{31}$-b-PBA$_{158}$	250 : 1 : 0.2	63	36500	1.14

The parameters determining the self-assembly such as the length of rods has been investigated earlier[25, 29] and the stirring rate during self-assembly was identified as an important aspect that can influence the rod length. As shown in Figure 1, a series of hard rods based on Poly(1-O-MAFru)$_{31}$-b-PMMA$_{166}$ with different aspect ratios were obtained at 25 ^{o}C by fine-tuning the stirring rates from 100-500 rpm. The lengths of rods are inversely proportional to the stirring rates with short rods being obtained at high stirring rates where the large shear rate leads to the scission of the rods in the process. In order to prepare soft rod-like micelles, Poly(1-O-MAFru)$_{31}$-b-PBA$_{158}$ which has a similar molecular weight to Poly(1-O-MAFru)$_{31}$-b-PMMA$_{166}$ was synthesized for self-assembly. Two soft rods with different aspect ratios were obtained with the same processing procedure. Once formed these aggregates were found to be stable against further aggregation if stored in the fridge.
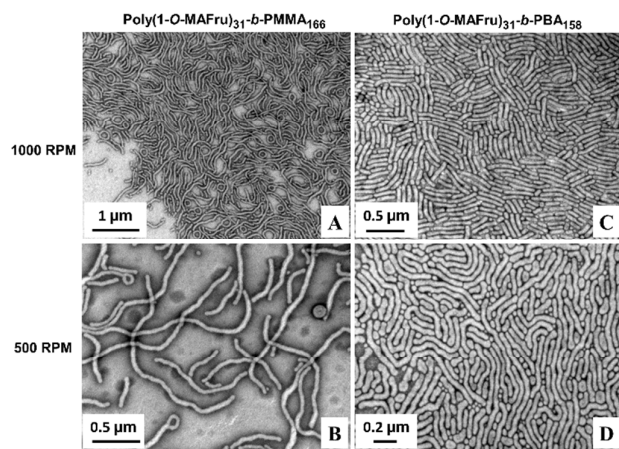

Figure 1. Rod-like micelles prepared from Poly(1-O-MAFru)$_{31}$-b-PMMA$_{166}$ and Poly(1-O-MAFru)$_{31}$-b-PBA$_{158}$; A: Poly(1-O-MAFru)$_{31}$-b-PMMA$_{166}$, 25°C, 1000 rpm; B: Poly(1-O-MAFru)$_{31}$-b-PMMA$_{166}$, 25°C, 500 rpm; C: Poly(1-O-MAFru)$_{31}$-b-PBA$_{158}$, 25°C, 1000 rpm; D: Poly(1-O-MAFru)$_{31}$-b-PBA$_{158}$, 25°C, 500rpm.

Although the focus of this work is to investigate of the effect of stiffness of the rod on cellular uptake, the influence of rod length needs to be considered as different rods may display different effects on cellular uptake. Therefore, to investigate the influence of rods stiffness on cellular uptake, the size of rods should be taken into account as well. The morphology and size of rod-like micelles were characterized by TEM and DLS. As shown in Figure S2 and Table 2, the length of rod-like micelles prepared from Poly(1-O-MAFru)$_{31}$-b-PMMA$_{166}$ are around 620 nm (A) and 1420 nm (B), respectively. However, rod-like micelles which are based on Poly(1-O-MAFru)$_{31}$-b-PBA$_{158}$ displayed shorter length when prepared under similar conditions (C: 310 nm and D: 450 nm). Despite several attempts, it was not possible to obtain cylindrical micelles using PBA with higher aspect ratios, probably due to the low glass transition temperature of the polymer that may have prevented the growth along the axis. Despite the differences in length in materials, it will later be evident that the aspect ratio has the least influence of all material properties.

Table 2. Size of rod-like micelles measured by DLS and TEM.

Sample	Glycopolymers	l_c^1 (nm)	D_h^2 (nm)	PDI
A	Poly(1-O-MAFru)$_{31}$-b-PMMA$_{166}$	620 ± 240	440 ± 90	0.15
B	Poly(1-O-MAFru)$_{31}$-b-PMMA$_{166}$	1420 ± 570	890 ± 450	0.29
C	Poly(1-O-MAFru)$_{31}$-b-PBA$_{158}$	310 ± 120	120 ± 2	0.11
D	Poly(1-O-MAFru)$_{31}$-b-PBA$_{158}$	450 ± 210	490 ± 290	0.23

lc^1: Contour length of rod-like micelles calculated from TEM images;

D_h^2: Hydrodynamic diameters measured by DLS.

The stiffness of the rods is quantitatively measured by AFM. As shown in Figure 2, rod-like micelles prepared from Poly(1-O-MAFru)$_{31}$-b-PBA$_{158}$ collapsed on the surface in dry state exhibiting significant deformation. In contrast, the deformation of rods based on Poly(1-O-MAFru)$_{31}$-b-PMMA$_{166}$ is negligible highlighting the higher structural integrity. The average DMT modulus calculation indicates that rods prepared from Poly(1-O-MAFru)$_{31}$-b-PMMA$_{166}$ (E = 2500 MPa, range between 0.5 to 5 GPa) are stiffer than those prepared from Poly(1-O-MAFru)$_{31}$-b-PBA$_{158}$ (average E = 350 MPa, range from 0.15 to 1.2 GPa). These results are in agreement with those in literature.[30] The moduli of rods are in the same range as those of bulk materials. The values obtained herein are comparable to the physical properties of the living nanoscopic organisms, namely viruses. Spherical viruses own Young's moduli that lie in the range of 100 and 2000 MPa in size.[31] Moreover the stiffness of the virus was found to change with maturation, which was observed to influence the cellular uptake.[32]

Before investigating the cellular uptake of rods by breast cancer cells, the fluorescence intensity of the nanoparticles was measured. Since fluorescein-O-methacrylate was added during the synthesis of the fructose block, which was subsequently chain extended using BA and MMA respectively, the obtained rod-like micelles have excitation and emission spectrum peak wavelengths of 490/530 nm respectively. As both hydrophobic blocks had similar molecular weights, the

fluorescence of all polymers used is comparable. As a result, all polymer solutions used here have similar fluorescence intensity, which facilitate the direct comparison in the cell uptake studies. However, as fluorescein tends to photobleach, the fluorescence intensity was tested prior to each

experiment. As shown in Figure S3, the fluorescein intensity of rod-like micelles prepared from Poly(1-O-MAFru)$_{31}$-b-PBA$_{158}$ with the emission peak maxima at 530 nm (FI = 610) is close to that of Poly(1-O-MAFru)$_{31}$-b-PMMA$_{166}$ (FI = 663).
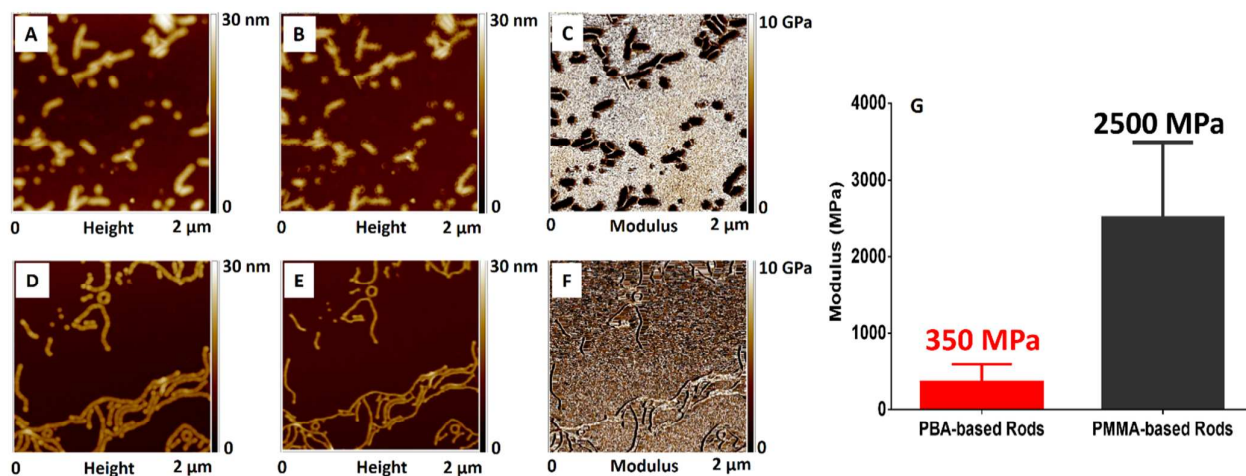

Figure 2. AFM profile of rod-like micelles. (A) topological image of rods prepared from Poly(1-O-MAFru)$_{31}$-b-PBA$_{158}$ (tapping mode); (B) topological image of rods prepared from Poly(1-O-MAFru)$_{31}$-b-PBA$_{158}$ (peakforce tapping with 3nN set point); (C) modulus image of rods prepared from Poly(1-O-MAFru)$_{31}$-b-PBA$_{158}$ (D) topological image of rods prepared from Poly(1-O-MAFru)$_{31}$-b-PMMA$_{166}$ (tapping mode); (E) topological image of rods prepared from Poly(1-O-MAFru)$_{31}$-b-PMMA$_{166}$ (peakforce tapping with 20 nN set point). (F) modulus image of rods prepared from Poly(1-O-MAFru)$_{31}$-b-PMMA$_{166}$; (G) DMT Moduli of rods calculated by AFM, PBA polymer is between 0.15 to 1.2 GPa and PMMA is between 0.5 to 5 GPa.

Confocal microscopy is a versatile tool to qualitatively compare the amount of endocytotic micelles by analyzing the fluorescence intensity of micelles inside the cells. The rod-like micelles in Table 2 were incubated with MCF-7 and MDA-MB-231. A high polymer concentration of 200 µg/mL was chosen to be added to the cell media as self-assembled structures are sensitive to disassembly. Lower concentration can lead to structural changes to the point of full disassembly into single block copolymers.[33] Cell growth media did not induce any morphology changes and no albumin adsorption on the surface was observed according to earlier studies.[5] As shown in Figure 3, both MCF-7 and MDA-MB-231 cells took up more stiff rods (Figure 3A and 3B) than soft ones (Figure 3C and 3D), regardless of the length difference. Even stiff rods with lengths of around 1420 nm can be internalized by cells. However, the amount of internalized short soft rods (310 nm) was negligible. The quantitative analysis of uptake was further conducted by flow cytometry (Figure 4). The results are consistent with those obtained from confocal microscopy. Both MCF-7 and MDA-MB-231 cells exhibit higher affinity to stiff rods than to soft ones, regardless of the rod length. Even short soft rods with a length of 310 nm (Rod C) have much less uptake than long stiff rods which have a mean length of 1420 nm (Rod B). However, the effect of the length on cellular uptake is obvious when the stiffness of rods is comparable. Both Rod A and Rod C exhibited higher uptake than their corresponding longer rods, which are in agreement with our former results that cellular uptake of rod-like micelles is affected by their length.[25]
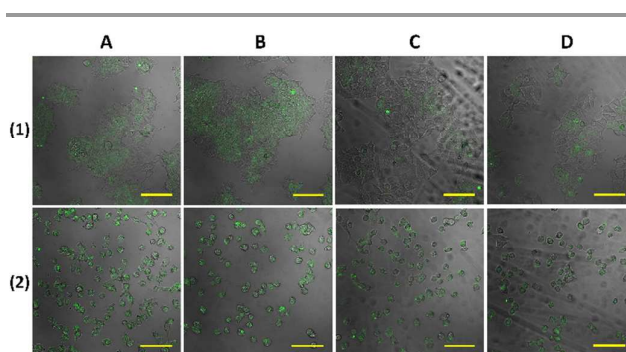

Figure 3. Cellular uptake of rod-like micelles by MCF-7 (1) and MDA-MB-231 cells (2) measured by laser scanning confocal microscopy. A: rods prepared from Poly(1-O-MAFru)$_{31}$-b-PMMA$_{166}$, l_c =620 nm; B: rods prepared from Poly(1-O-MAFru)$_{31}$-b-PMMA$_{166}$, l_c =1420 nm; C: rods prepared from Poly(1-O-MAFru)$_{31}$-b-PBA$_{158}$, l_c =310 nm; D: rods prepared from Poly(1-O-MAFru)$_{31}$-b-PBA$_{158}$, l_c =450 nm. The images were merged with DIC (differential interference contrast) images. Scale bars (confocal microscopic images) = 100 µm.

The stiffness effect of spherical nanoparticles on cellular uptake has been recently reported. Yi *et al*. built a theoretical model based on Helfrich's theory to analyze the cellular uptake of a fluid vesicular nanoparticle such as liposome.[34] Their results revealed that cellular uptake is very sensitive to the relative stiffness of nanoparticles compared to the cell membrane. Soft vesicles are less likely to be fully wrapped by the cell membrane than stiff nanoparticles. Similar results have recently been obtained by Sun *et al*.[35] They correlated the stiffness of core-shell nanoparticles with a lipid shell on the cell

uptake and found that stiff nanoparticles were able to pass more easily through cell membranes. Simulations revealed that the deformation of soft nanoparticles is energetically unfavorable for cellular uptake. The stiffness effect has also been observed by Yi *et al.* in the cellular uptake of solid nanocapsules and fluid vesicular nanoparticles.[36] They conducted a theoretical study and found that fluid vesicular nanoparticles require more adhesion energy to achieve fully wrapping than solid nanocapsules with the same bending stiffness. The explanation to the stiffness effect on cellular uptake was proposed by Zhang *et al.*[37] They postulated that the softness of nanoparticles may affect the wetting angle and the extent of the nanoparticle spreading on the cell membrane. Compared with stiff nanoparticles, soft ones have larger wetting angle and higher spreading extent on the cell membrane. This behavior was confirmed with the two types of rods here as the soft rod clearly loses its shape on hard surfaces as shown in Figure 2. Large curvatures at the spreading front will be formed by the highly spread soft nanoparticles. A large bending energy barrier which may be sufficient to stall the wrapping has to be overcome by nanoparticles for further wrapping.

Figure 4. Cellular uptake of rod-like micelles by MCF-7 and MDA-MB-231 cells measured by flow cytometry. (1) cell count vs log of normalized fluorescence at 530 nm; (2) mean fluorescence intensity (MFI) of cells after internalization of nanoparticles. A: rods prepared from Poly(1-*O*-MAFru)$_{31}$-*b*-PMMA$_{166}$, l_c =620 nm; B: rods prepared from Poly(1-*O*-MAFru)$_{31}$-*b*-PMMA$_{166}$, l_c =1420 nm; C: rods prepared from Poly(1-*O*-MAFru)$_{31}$-*b*-PBA$_{158}$, l_c =310 nm; D: rods prepared from Poly(1-*O*-MAFru)$_{31}$-*b*-PBA$_{158}$, l_c =450 nm.

Though endocytosis mechanism of nanoparticles have been extensively discussed,[38-40] knowledge on the influence of rod stiffness on cellular uptake is limited. This is partially due to the complexity of endocytosis during internalization of rod-like nanoparticles. In addition, the narrow compositional space of rods preparation also makes it challenging to fabricate rod-like nanoparticles with uniform size and shape. However, the endocytosis model of rod-like micelles has been extensively discussed. Discher *et al.* proposed that biotinylated soft worm-

like micelles can be internalized by receptor mediated endocytosis either through packaging of the micelles or by fragmentation of the rod.[41] The group investigated in addition the flow effect on endocytosis by steady flow of rod-like micelles and spherical vesicles past phagocytes.[42] Spherical vesicles were prone to cell adhesion and appeared to be taken up by the cell straight after cell contact while rod-like micelles were easily detached from phagocytes. Interestingly, fragments, generated from the end-cap of cylindrical micelle, were observed to be taken up by cells. This observation suggested that the fragmentation of rod-like micelles may take place at the end-caps of rods under strong hydrodynamic force. The pivotal role of rod end-caps in cellular uptake via phagocytosis has been confirmed by other groups. Successful uptake of stiff rod-like nanoparticles was only observed when the contact point between cell membrane and nanoparticles was at the end-caps of rods.[17] This phenomenon is similar to the salient strategy which is widely used by filamentous bacteria to protect themselves from macrophage attack.[43, 44] In a proof-of concept experiment, filamentous *E. coli* bacteria was found to be internalized successfully by macrophages only when one of the terminal bacterial filament poles was accessible to macrophages.[45] Therefore, effective contact between cell membrane and end-caps of rods may be prerequisite for successful internalization of rod-like nanoparticles. Simulations have recently been employed to understand the cellular uptake of nanoparticles. Coarse-grained (CG) methods, which have gained great popularity for their flexibility and diversity, are versatile tools to analyze the interactions on the molecular level and nanoparticle absorption/uptake by cells at the subcellular level.[37] Huang *et al.* adopted the one-agent-thick membrane model to investigate the endocytosis process of spherical-ended rod-like nanoparticles.[46] In these simulations, the cylindrical nanoparticles were initially docked on the membrane with their long axes perpendicular to the membrane surface. However, different entry modes were observed in the wrapping process of nanoparticles. Rod-like nanoparticles with aspect ratio of 1.5 tilted by an angle of around 20° from initial upright docking position once wrapping starts keeping this angle until the nanoparticle was fully internalized. The wrapping process of nanoparticles with a larger aspect ratio (ρ = 2) usually underwent a lying-down-then-standing-up sequence. For rod-like nanoparticles with the long axis parallel to the membrane surface, the nanoparticle would arrange perpendicular to the cell membrane and then be internalized. The lying-down-then-standing-up sequence is consistent with the results reported by Shi *et al.*[47] They used CGMD simulations as well as corresponding experimental observations for capped multi-walled carbon nanotubes endocytosis. Their results demonstrated that at a relatively low receptor density the nanotube rotated and is internalized with an entry angle around 90°, exhibiting a tip-entry phenomenon. Though the receptor-mediated endocytosis of short nanorods just displayed a single interaction mode of a lying-down-then-standing-up sequence, that of long cylindrical nanoparticles are reported to exhibit two interaction modes: perpendicular
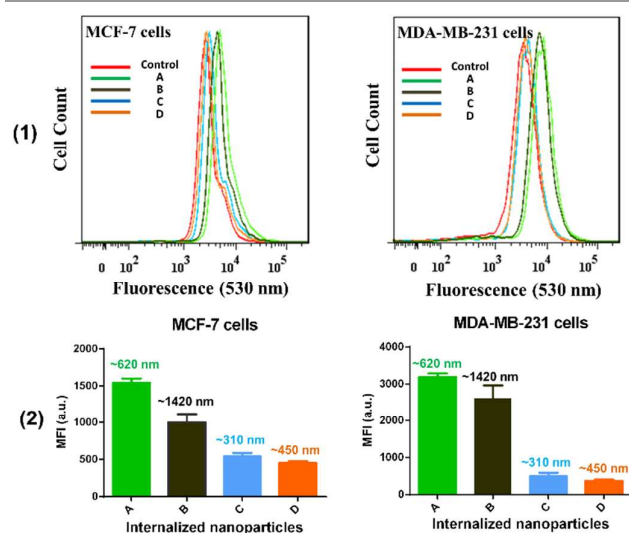
entry mode and parallel adhering mode.[48] These two modes are dependent on the normalized membrane tension $\bar{\sigma} = 2\sigma R^2/B$, where R is the radius of 1D nanomaterials. When $\bar{\sigma}$ is below a critical value $\bar{\sigma}_c$, the internalization is dominated by the membrane bending energy and the entry of 1D nanomaterial is in a high entry angle. If $\bar{\sigma} > \bar{\sigma}_c$, the stretching energy dominates over the membrane bending energy and the nanomaterial is in a low entry angle and eventually adheres to the membrane surface in a near-parallel configuration.
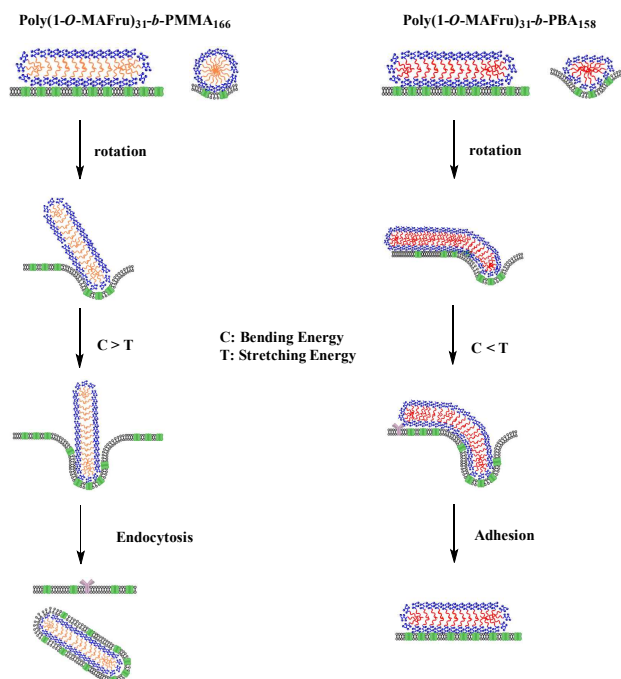
Scheme 2. Proposed cellular uptake process of rod-like micelles by MCF-7cells.

Based on the discussion above, we propose a mechanism for the endocytosis process of rod-like micelles with different stiffness. Since all rod-like micelles in this work were prepared from fructose-based glycopolymers,[5] the internalization of these nanoparticles follow receptor-mediated endocytosis mechanism as reported.[16] In receptor-mediated endocytosis, the wrapping process is limited by the diffusion of receptors in the cell membrane toward the contact region.[49] The end-caps of rod-like micelles should be wrapped first, rather than the lateral walls because the wrapping of the curved end-caps is governed by 2D diffusion of receptors in the membrane plane while that of cylindrical wall is regulated by 1D diffusion of receptors.[37] Once the membrane deformation energy penalty induced by wrapping the end-caps was overcome by the specific receptor-ligand interaction, the subsequent interaction was controlled by the two tension-dependent interaction modes.[48] These two modes are dependent on a single dimensionless parameter, the normalized membrane tension $\bar{\sigma}$. The tension $\bar{\sigma}$ can be regarded as the relative fraction of membrane stretching and bending energies in comparison to the total elastic energy of the membrane.[37] When membrane bending energy dominates over the

stretching energy, rod-like nanoparticles will be rotated by the membrane to a perpendicular entry angle for wrapping. However, when the rods are driven by the stretching energy, a low entry angle is favorable and rod-like micelles eventually adhere to the membrane surface in a near-parallel configuration. Based on this, the cellular uptake of both two rods is proposed to follow a three-step process. When soft rods, which were prepared from Poly(1-O-MAFru)$_{31}$-b-PBA$_{158}$, dock on the membrane, they spread on the cell membrane and form a large wetting angle. Large curvatures at the spreading front will form a large bending energy barrier. In this case, the membrane stretching energy dominates over the bending energy and nanoparticles eventually adhere to the membrane surface. However, during the wrapping of stiff rods, which were generated from Poly(1-O-MAFru)$_{31}$-b-PMMA$_{166}$, membrane bending energy dominates over the stretching energy and nanoparticles will be internalized in a perpendicular entry angle. The hypothesized cellular uptake mechanism is summarized in Scheme 2.
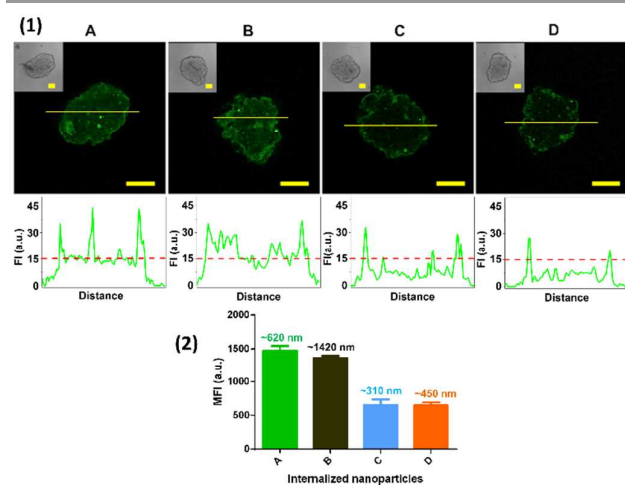

Figure 5. Penetration of rod-like micelles in 3D MCTS observed with confocal microscopy. (1) Selective uptake of rods of different size by MCF-7 spheroids and relative fluorescence (FI) distribution at the perimeter and the bulk of the spheroids; the inserts are the DIC images of the spheroids. Scale bar = 200 μm. (2) Mean fluorescence intensities (MFI) of confocal microscopic images in (1). A: rods prepared from Poly(1-O-MAFru)$_{31}$-b-PMMA$_{166}$, l_c =620 nm; B: rods prepared from Poly(1-O-MAFru)$_{31}$-b-PMMA$_{166}$, l_c =1420 nm; C: rods prepared from Poly(1-O-MAFru)$_{31}$-b-PBA$_{158}$, l_c =310 nm; D: rods prepared from Poly(1-O-MAFru)$_{31}$-b-PBA$_{158}$, l_c =450 nm.

3D multicellular spheroids, which is an excellent model resemble to in vivo tumors, have also been used to investigate the effect of rod stiffness on cellular uptake and penetration. As shown in Figure 5, the confocal microscopy results reveal that stiff rods exhibit deeper penetration into 3D spheroids than soft ones. Most of the soft rods accumulated on the peripheral layer of the spheroids. These results are consistent with our former study, in which the penetration of micelles was found to be dependent more on transcellular transport than on diffusion through extracellular matrices between the cells.[27] The unfavorable uptake of soft rods by cells on the peripheral layer inhibited the further penetration of nanoparticles to the core of spheroids. Most importantly, the

long hard nanoparticle had a superior performance compared to the soft ones. Although soft and hard nanoparticles of comparable aspect ratios were not generated in this work, these results indicate that the hardness is overpowering and chain length dependency of cellular uptake.

Since rod-like micelles have potential advantage as compared to spherical counterparts in terms of circulation time,[42] some reports have tried to load drugs into these cylindrical nanoparticles.[50-53] However, drug induced morphology transition, in which rod-like or spherical micelles changed to other shapes when hydrophobic drugs were loaded, is frequently observed.[54, 55] It is reported the morphologies of drug loaded micelles are significantly affected by several factors such as structure of additives,[52] block copolymers type[55] and the linking between loaded drugs and micelles core (physical encapsulation or chemical conjugation).[51, 56] Therefore, the morphological stability of rod-like micelles during drug-loading and cellular uptake process is crucial for their further use as drug carriers in nano-medicine. To enhance stability, some cross-linked rod-like micelles have been designed.[6] In addition, the method used for drug encapsulation also plays an important role. Well-defined paclitaxel-loaded rod-like micelles have been prepared successfully via a post-loading method.[16, 53] Thus, it is possible to load drugs inside rod-like micelles but further study on the drug location inside the rod-like micelles is still needed in order to maintain their cylindrical morphologies as well as high drug loading capacity for biomedicine applications.

Conclusions

In this research, fructose-coated rod-like micelles of different length and stiffness were prepared successfully by fine-tuning the processing parameters like stirring rate and temperature during self-assembly. The stiffness of different rods were measured by AFM and the results indicate that rods prepared from Poly(1-O-MAFru)$_{31}$-b-PMMA$_{166}$ are much harder than those prepared from Poly(1-O-MAFru)$_{31}$-b-PBA$_{158}$. Cellular uptake of these different rod-like micelles by breast cancer cells in 2D and 3D models indicate that internalization of rod-like micelles is significantly affected by the stiffness of micelles, though lengths of rods also play an important role. Based on these results, we proposed the endocytosis mechanism of soft and hard rods. Our results revealed that hard rods are more likely to be taken up by breast cancer cells than soft rods.

Conflicts of interest

There are no conflicts to declare.

Acknowledgements

References

1. K. Kataoka, A. Harada and Y. Nagasaki, *Adv. Drug Deliv. Rev.*, 2001, **47**, 113-131.
2. B. D. Chithrani, A. A. Ghazani and W. C. Chan, *Nano Lett.*, 2006, **6**, 662-668.
3. W. Jiang, B. Y. Kim, J. T. Rutka and W. C. Chan, *Nat. Nanotechnol.*, 2008, **3**, 145-150.
4. S. Zhang, J. Li, G. Lykotrafitis, G. Bao and S. Suresh, *Adv.Mater.*, 2009, **21**, 419-424.
5. J. Zhao, K. Babiuch, H. Lu, A. Dag, M. Gottschaldt and M. H. Stenzel, *Chem. Commun.*, 2014, **50**, 15928-15931.
6. K. Zhang, H. Fang, Z. Chen, J.-S. A. Taylor and K. L. Wooley, *Bioconjugate Chem.*, 2008, **19**, 1880-1887.
7. Y. Li, M. Kroger and W. K. Liu, *Nanoscale*, 2015, **7**, 16631-16646.
8. O. Shimoni, Y. Yan, Y. Wang and F. Caruso, *ACS Nano*, 2013, **7**, 522-530.
9. J. M. Bergen, H. A. Von Recum, T. T. Goodman, A. P. Massey and S. H. Pun, *Macromol. Biosci.*, 2006, **6**, 506-516.
10. H. Yuan, J. Li, G. Bao and S. Zhang, *Phys. Rev. Lett.*, 2010, **105**, 138101.
11. D. Li, Z. Tang, Y. Gao, H. Sun and S. Zhou, *Adv. Funct. Mater.*, 2016, **26**, 66-79.
12. T. Chen, X. Guo, X. Liu, S. Shi, J. Wang, C. Shi, Z. Qian and S. Zhou, *Adv. Healthc. Mater.*, 2012, **1**, 214-224.
13. Y. Gao, J. Zhao, X. Zhang, X. Wei, X. Xiong, X. Guo and S. Zhou, *J. Mater. Chem. B*, 2017, **5**, 4943-4954.
14. N. P. Truong, M. R. Whittaker, C. W. Mak and T. P. Davis, *Expert Opin. Drug Deliv.*, 2015, **12**, 129-142.
15. S. Venkataraman, J. L. Hedrick, Z. Y. Ong, C. Yang, P. L. R. Ee, P. T. Hammond and Y. Y. Yang, *Adv. Drug Deliv. Rev.*, 2011, **63**, 1228-1246.
16. J. Zhao, H. Lu, S. Wong, M. Lu, P. Xiao and M. H. Stenzel, *Polym. Chem.*, 2017, **8**, 3317-3326.
17. J. A. Champion and S. Mitragotri, *Pharm. Res.*, 2009, **26**, 244-249.
18. K. Zhang, R. Rossin, A. Hagooly, Z. Chen, M. J. Welch and K. L. Wooley, *J. Polym. Sci. Part A: Polym. Chem.*, 2008, **46**, 7578-7583.
19. F. E. Alemdaroglu, N. C. Alemdaroglu, P. Langguth and A. Herrmann, *Macromol. Rapid Commun.*, 2008, **29**, 326-329.
20. B. Karagoz, L. Esser, H. T. Duong, J. S. Basuki, C. Boyer and T. P. Davis, *Polym. Chem.*, 2014, **5**, 350-355.
21. A. Dag, J. Zhao and M. H. Stenzel, *ACS Macro Lett.*, 2015, **4**, 579-583.
22. T. J. Merkel, S. W. Jones, K. P. Herlihy, F. R. Kersey, A. R. Shields, M. Napier, J. C. Luft, H. Wu, W. C. Zamboni, A. Z. Wang, J. E. Bear and J. M. DeSimone, *Proc. Natl. Acad. Sci. U.S.A*, 2011, **108**, 586-591.
23. A. Dag, M. Callari, H. Lu and M. H. Stenzel, *Polym. Chem.*, 2016, **7**, 1031-1036.
24. C. von der Ehe, A. Rinkenauer, C. Weber, D. Szamosvari, M. Gottschaldt and U. S. Schubert, *Macromol. Biosci.*, 2016, **16**, 508-521.
25. J. Zhao, H. Lu, P. Xiao and M. H. Stenzel, *ACS Appl. Mat. Interfaces*, 2016, **8**, 16622-16630.
26. J. Rejman, V. Oberle, I. S. Zuhorn and D. Hoekstra, *Biochem.J.*, 2004, **377**, 159-169.

         ARTICLE

27. H. Lu, R. H. Utama, U. Kitiyotsawat, K. Babiuch, Y. Jiang and M. H. Stenzel, *Biomater. Sci.*, 2015, **3**, 1085-1095.

28. Y. Mitsukami, M. S. Donovan, A. B. Lowe and C. L. McCormick, *Macromolecules*, 2001, **34**, 2248-2256.

29. J. Zhao and M. H. Stenzel, in *Controlled Radical Polymerization: Materials*, American Chemical Society, 2015, vol. 1188, ch. 7, pp. 91-105.

30. M. Griepentrog, G. Krämer and B. Cappella, *Polym. Test.*, 2013, **32**, 455-460.

31. W. H. Roos, R. Bruinsma and G. J. L. Wuite, *Nat. Phys.*, 2010, **6**, 733-743.

32. N. Kol, M. Gladnikoff, D. Barlam, R. Z. Shneck, A. Rein and I. Rousso, *Biophys. J.*, 2006, **91**, 767-774.

33. Y. Kim, M. H. Pourgholami, D. L. Morris and M. H. Stenzel, *Biomacromolecules*, 2012, **13**, 814-825.

34. X. Yi, X. Shi and H. Gao, *Phys. Rev. Lett.*, 2011, **107**, 098101.

35. J. Sun, L. Zhang, J. Wang, Q. Feng, D. Liu, Q. Yin, D. Xu, Y. Wei, B. Ding and X. Shi, *Adv. Mater.*, 2015, **27**, 1402-1407.

36. X. Yi and H. Gao, *Soft Matter*, 2015, **11**, 1107-1115.

37. S. Zhang, H. Gao and G. Bao, *ACS Nano*, 2015, **9**, 8655-8671.

38. J. Zhao and M. H. Stenzel, *Polym. Chem.*, 2018, **9**, 259-272.

39. G. Sahay, D. Y. Alakhova and A. V. Kabanov, *J. Control. Release*, 2010, **145**, 182-195.

40. S. E. A. Gratton, P. A. Ropp, P. D. Pohlhaus, J. C. Luft, V. J. Madden, M. E. Napier and J. M. DeSimone, *Proc. Natl. Acad. Sci. U.S.A*, 2008, **105**, 11613-11618.

41. P. Dalhaimer, A. J. Engler, R. Parthasarathy and D. E. Discher, *Biomacromolecules*, 2004, **5**, 1714-1719.

42. Y. Geng, P. Dalhaimer, S. Cai, R. Tsai, M. Tewari, T. Minko and D. E. Discher, *Nat. Nanotechnol.*, 2007, **2**, 249-255.

43. S. S. Justice, D. A. Hunstad, L. Cegelski and S. J. Hultgren, *Nature Rev. Microbiol.*, 2008, **6**, 162-168.

44. A. A. Brakhage, S. Bruns, A. Thywissen, P. F. Zipfel and J. Behnsen, *Curr. Opin. Microbiol.*, 2010, **13**, 409-415.

45. J. Möller, T. Luehmann, H. Hall and V. Vogel, *Nano Lett.*, 2012, **12**, 2901-2905.

46. C. Huang, Y. Zhang, H. Yuan, H. Gao and S. Zhang, *Nano Lett.*, 2013, **13**, 4546-4550.

47. X. Shi, A. von dem Bussche, R. H. Hurt, A. B. Kane and H. Gao, *Nat. Nanotechnol.*, 2011, **6**, 714-719.

48. X. Yi, X. Shi and H. Gao, *Nano Lett.*, 2014, **14**, 1049-1055.

49. H. Gao, W. Shi and L. B. Freund, *Proc. Natl. Acad. Sci. USA*, 2005, **102**, 9469-9474.

50. X. Wan, Y. Min, H. Bludau, A. Keith, S. S. Sheiko, R. Jordan, A. Z. Wang, M. Sokolsky-Papkov and A. V. Kabanov, *ACS Nano*, 2018, **12**, 2426-2439.

51. Y. Wang, D. Wang, Q. Fu, D. Liu, Y. Ma, K. Racette, Z. He and F. Liu, *Mol. Pharm.*, 2014, **11**, 3766-3771.

52. M. Khimani, R. Ganguly, V. K. Aswal, S. Nath and P. Bahadur, *J. Phys. Chem. B*, 2012, **116**, 14943-14950.

53. S. Cai, K. Vijayan, D. Cheng, E. M. Lima and D. E. Discher, *Pharm. Res.*, 2007, **24**, 2099-2109.

54. A. Schulz, S. Jaksch, R. Schubel, E. Wegener, Z. Di, Y. Han, A. Meister, J. Kressler, A. V. Kabanov, R. Luxenhofer, C. M. Papadakis and R. Jordan, *ACS Nano*, 2014, **8**, 2686-2696.

55. Z. Zhou, A. D'Emanuele and D. Attwood, *Int. J. Pharm.*, 2013, **452**, 173-179.

56. A. S. Mikhail and C. Allen, *Biomacromolecules*, 2010, **11**, 1273-1280.

Length *vs* stiffness, which plays a dominant role in the cellular uptake of fructose-based rod-like micelles by breast cancer cells in 2D and 3D cell culture models?

Jiacheng Zhao,[a,b] Hongxu Lu,[a,b] Yin Yao,[c] Sylvia Ganda,[a,b] and Martina H. Stenzel †[a,b]

[a]Centre for Advanced Macromolecular Design, [b]School of Chemistry, [c]Electron Microscope Unit, The University of New South Wales, Sydney, Australia.

TABLE OF CONTENT
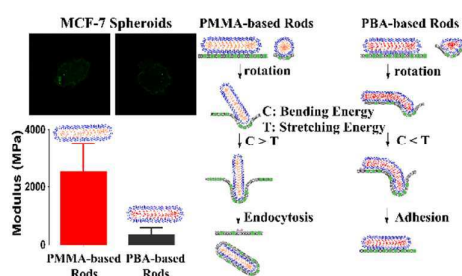
Internalization of rod-like micelles by breast cancer cells is significantly affected by the stiffness of nano-rods.